Strong Coupling Between Nanofluidic Transport and Interfacial Chemistry: How Defect Reactivity Controls Liquid-Solid Friction Through Hydrogen Bonding

Laurent Joly,[*,†] Gabriele Tocci,[‡,¶] Samy Merabia,[†] and Angelos Michaelides[‡]

†Institut Lumière Matière, UMR5306 Université Lyon 1-CNRS, Université de Lyon 69622 Villeurbanne, France

‡Thomas Young Centre, London Centre for Nanotechnology, and Department of Physics and Astronomy, University College London, London WC1H 0AJ, United Kingdom

¶Current address: Laboratory for fundamental BioPhotonics, Institute of Bioengineering, School of Engineering, École Polytechnique Fédérale de Lausanne, CH-1015, Lausanne, Switzerland and Laboratory of computational Science and Modelling, Institute of Materials, School of Engineering, École Polytechnique Fédérale de Lausanne, CH-1015, Lausanne, Switzerland.

E-mail: laurent.joly@univ-lyon1.fr

Abstract

Defects are inevitably present in nanofluidic systems, yet the role they play in nanofluidic transport remains poorly understood. Here, we report ab initio molecular dynamics (AIMD) simulations of the friction of liquid water on defective graphene and boron nitride sheets. We show that water dissociates at certain defects and that these "reactive" defects lead to much larger friction than the "non-reactive" defects at which water molecules remain intact. Furthermore, we find that friction is extremely sensitive to the chemical structure of reactive defects and to the number of hydrogen bonds they can partake in with the liquid. Finally, we discuss how the insight obtained from AIMD can be used to quantify the influence of defects on friction in nanofluidic devices for water treatment and sustainable energy harvesting. Overall, we provide new insight into the role of interfacial chemistry on nanofluidic transport in real, defective systems.

Graphical TOC Entry
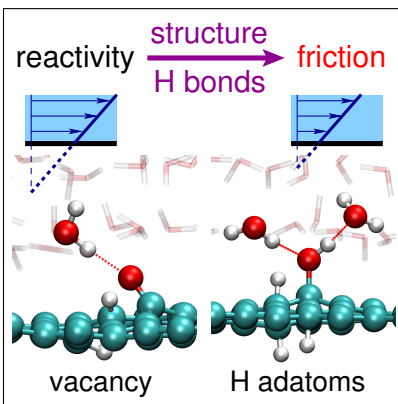
Nanofluidic transport plays a key role in numerous present-day applications, including water treatment and sustainable energies, where new two-dimensional materials offer promise of radical performance improvement.[1–4] For instance, carbon nanotube membranes and nanoporous graphene can filter water with an excellent permeability to selectivity ratio.[5–7] It has also been shown recently that nanofluidic systems based on boron nitride (BN) nanotubes can harvest the so-called blue energy (*i.e.*, the osmotic energy of salt water) with unprecedented efficiency.[8] However, transport efficiency in state-of-the-art artificial nanofluidic devices is still far from optimal, and well below the performance of biological systems.[9,10] In order to improve the efficiency of nanofluidic systems, it is crucial to understand the specific details of nanoscale transport. In particular, surfaces and interfaces play an increasingly prominent role when the system size is reduced, so that at the nanoscale transport is essentially controlled by surface effects.[11] For instance, nanoscale flows are limited by interfacial hydrodynamics, and can be enhanced by liquid-solid slip[12,13] arising from low liquid-solid friction.[14] Electrokinetic effects, which couple different types of transport (hydrodynamic, ionic, thermal. . .) at surfaces, key to nanofluidic energy conversion systems,[11,15,16] are also strongly affected by liquid-solid slip.[17–24]

Interfacial hydrodynamics and friction are sensitive to the molecular detail of the interface,[12] e.g., to the presence of defects on solid surfaces – typically created during growth or synthesis.[25–28] Defects can even be desirable for nanofluidic energy conversion, since the efficiency of the conversion is directly related to the surface charge,[11,20,29] usually found in the form of charged defects. Defects can be reactive,[30–33] and although previous work has investigated how reactive defects modify the structure of the water-solid interface,[34–37] the consequences of this reactivity on nanofluidic transport remains an open question. Indeed, up to now only the direct, mechanical effect of defects on liquid-solid friction has been explored using simulation approaches based on force field molecular dynamics.[38,39] At the same time, recent work shows that it is now possible to explore hydrodynamics of confined liquids with *ab initio* molecular dynamics (AIMD), *i.e.* molecular dynamics simulations where forces are

obtained from electronic structure calculations.[14,40] In particular, we have recently shown that liquid-solid friction coefficients can be computed directly from *ab initio* simulations, from which specific electronic structure effects on friction were revealed.[14]

Here we use AIMD to investigate how defects and defect reactivity affect nanofluidic transport. We focus on carbon and BN surfaces, as they show great promise for nanofluidic applications, related in particular to their ultralow liquid/solid friction, which could be threatened by defects. We show that defect reactivity to water is key to the friction increase, with non-reactive defects having a negligible influence, and reactive defects being highly detrimental. We also find that friction depends on the number of hydrogen bonds the defects make with water, so that it can be quite different for reactive defects with a similar size but different structure. We then discuss the consequences of our results for water permeability in experimental (defective) nanostructures, and for applications in nanofluidic energy conversion. Overall we show here that there is very strong coupling between nanofluidic transport and interfacial chemistry in carbon and BN systems, which depends dramatically on the chemical nature of the defects and their ability to partake in hydrogen bonding with the liquid.

We performed AIMD simulations of a thin liquid water film on graphene and on a single layer of hexagonal BN, carrying different types of defects. The computational setup, detailed in the supporting information (SI), is based on the one used in Ref. 14, where the friction of water on pristine graphene and BN was investigated. In particular, we performed Born-Oppenheimer molecular dynamics with the CP2K code;[41] the forces were computed at the density functional theory (DFT) level, using the optB88-vdW exchange-correlation functional.[42] This functional was shown to describe with a good accuracy both liquid water[43] and soft layered materials such as graphite and BN.[44] As compared to reference quantum Monte Carlo data,[45–47] it slightly overbinds water to graphene and BN, but the relative energy differences between different sites (relevant to friction) are well described (see the SI of Ref.[14]). There are, of course, many types of defects that we could examine. However, AIMD

4

is very demanding and we had to select a small set of common, representative defects.[25–28]

We introduced three different defects in the graphene sheets (Fig. 1). Firstly, as an example
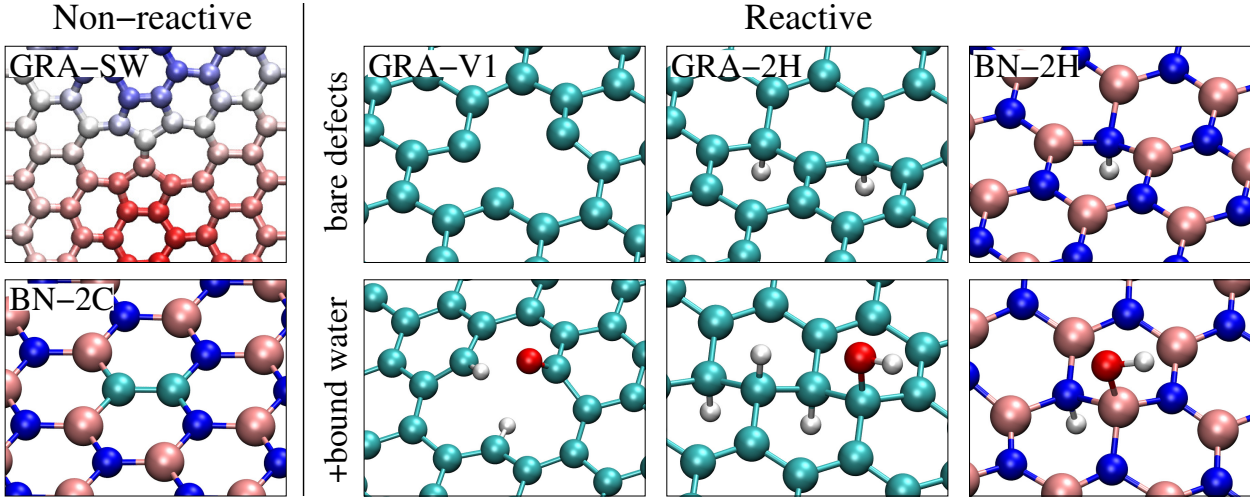

Figure 1: Top views of the defects introduced in graphene and boron nitride (BN). Left) Non-reactive defects: "GRA-SW" – graphene with a Stone-Wales defect, a simple topological defect that induces a corrugation of the sheet;[48] atoms are colored according to their height, from red (lower) to blue (higher); "BN-2C" – BN with 2 adjacent B and N atoms substituted by 2 C atoms. Right) Reactive defects, before contact with water (top) and with a bound dissociated water molecule (bottom): "GRA-V1" – a carbon monovacancy in graphene; "GRA-2H" – two H adatoms on graphene; "BN-2H" – one of two H adatoms well separated on a BN sheet (full system is represented in the supporting information). Except for the GRA-SW defect, carbon, boron, nitrogen, oxygen and hydrogen atoms are colored in cyan, magenta, blue, red and white, respectively.

of a topological defect, we simulated a Stone-Wales (SW) defect in a *ca.* $2.5 \times 2.5\,\mathrm{nm^2}$ sheet.

SW defects can be formed during the production of carbon nanostructures, and have been

imaged in transmission electron microscopy.[49] We also considered two other common point

defects (using a smaller, *ca.* $1.3 \times 1.3\,\mathrm{nm^2}$ sheet): a monovacancy – denoted V1, and a

simple example of an adatom defect consisting of two adsorbed hydrogen atoms – denoted

2H. The latter defect can typically appear during the production of carbon nanostructures

using hydrogenated gases.[50] Finally, we considered defective BN, using a *ca.* $1.3 \times 1.3\,\mathrm{nm^2}$

cell (see Fig. 1 and Fig. S1 in the SI). Firstly, in order to investigate the effect of doping BN

nanostructures with carbon, we substituted two adjacent boron and nitrogen atoms by two

carbon atoms (2C defect). We introduced two 2C defects in the simulated sheet. Secondly,

similar to the graphene sheet, we introduced two hydrogen atoms bonded to well separated nitrogen atoms (2H defect).

We started by investigating the defect reactivity to water, by exploring the tendency of water molecules to dissociate at the defects, in the absence of a water film. To that aim, we relaxed various possible configurations with a water molecule dissociated at the defects and computed the binding energy, defined as the energy difference between the relaxed structure and a water molecule fully separated from the defective sheet. On the GRA-SW and the BN-2C defects, we could not find any energetically favorable dissociated state. We will therefore describe these two defects as "non-reactive" to water. On the other hand, we found that water dissociation was energetically favorable on the GRA-V1 and the GRA-2H defects, with binding energies of *ca.* 4.0 eV and *ca.* 0.8 eV, respectively. Fig. 1 shows the most stable structures identified. In the vacancy case, water fully dissociates,[31,32] i.e. the oxygen and the two hydrogens bind to the three carbon atoms surrounding the vacancy. In the case of the 2H defect, the water molecule dissociates to form an OH and an H group. Previous work has shown that water dissociates at the BN-2H defect in vacuum.[8] Here we took a step further and performed an AIMD simulation of a water film on a BN-2H sheet, and we observed a spontaneous dissociation event; as with the GRA-2H system, an OH and an H group were formed (see Fig. S1 in the SI). In the following we refer to the GRA-V1, GRA-2H and BN-2H defects as "reactive".

After the defect reactivity had been characterized, we studied with AIMD how this selection of defects affected the friction of liquid water. In order to build the initial configurations for the AIMD simulations, we placed *ca.* 2 nm water films on top of the optimized structures of the defective sheets (*i.e.*, including the dissociated water molecule for reactive defects), and pre-equilibrated the systems using force field molecular dynamics. We imposed periodic boundary conditions in all directions (with a vacuum gap of *ca.* 15Å between the periodic images along the normal to the interface), so that both the liquid film and the graphene/BN sheet were free to diffuse along the interface. No further chemical reaction between the

6

water film and the sheets was observed during the subsequent AIMD simulations. We then computed the liquid-solid friction coefficient λ, relating the interfacial friction force F at a slipping interface to the slip velocity v_{slip}, *i.e.*, the tangential velocity jump at the interface: $F = \lambda \mathcal{A} v_{\text{slip}}$, with $\mathcal{A}$ the area of contact.[12,51,52] In the framework of linear response theory, λ can be obtained from the equilibrium fluctuations of the friction force, using a Green-Kubo relation:[53,54]

$$\lambda = \frac{1}{\mathcal{A} k_{\text{B}} T} \int_0^\infty \langle F(t) F(0) \rangle \, \mathrm{d}t, \tag{1}$$

where k_{B} is the Boltzmann constant and T the temperature. In previous work,[14] we performed a number of AIMD and force field MD simulations to ensure that the friction coefficients extracted from AIMD were not affected by the length of the AIMD trajectory and by the size of the system. Here, a discussion on the validity of our results for the friction coefficient in the particular case of defective sheets is reported in sections 3.2 to 3.4 of the SI. In order to confirm the results of the friction calculations with Eq. (1), and following a similar approach applied to the measure of thermal conductance,[55] we also estimated the friction coefficient using an alternative Green-Kubo formula involving the initial slope of the autocorrelation function of the slip velocity fluctuations at equilibrium, $C_{vv} = \langle v_{\text{slip}}(t) v_{\text{slip}}(0) \rangle$:

$$\lambda = -\frac{m_{\text{eff}}^2}{\mathcal{A} k_{\text{B}} T} \left. \frac{\mathrm{d} C_{vv}}{\mathrm{d}t} \right|_{t=0^+}, \tag{2}$$

where m_{eff} is the effective mass of the liquid-solid system, given by $m_{\text{eff}} = m_{\text{liq}} m_{\text{sol}} / (m_{\text{liq}} + m_{\text{sol}})$, m_{liq} and m_{sol} being the liquid and solid mass, respectively. As detailed in the SI, Eq. (2) can be derived from a Langevin equation describing the relative Brownian motion of the liquid film with regard to the solid surface. We will therefore refer to this new approach as the "Langevin" method in the following.

Figure 2 presents the computed friction coefficients for the 5 defects considered, using the standard and alternative Green-Kubo formulae. Both methods provide consistent values and comparable statistical uncertainties. Figure 2 reveals a strong contrast between reactive
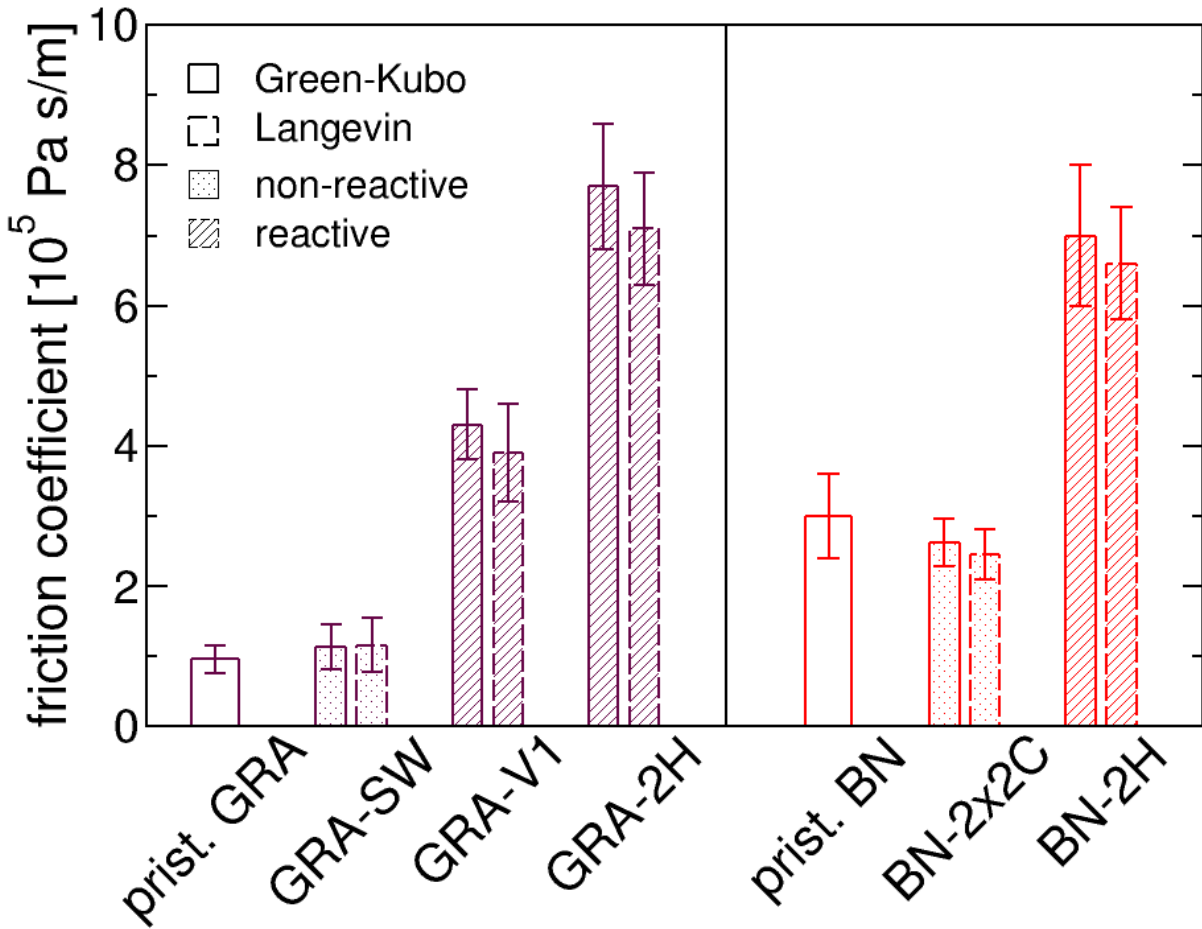
Figure 2: Green-Kubo and Langevin estimates of the friction coefficient for the various systems considered. The pristine graphene (prist. GRA) and boron nitride (prist. BN) values are taken from Ref. 14. Error bars have been obtained by block averaging the data. It can be seen that for defects at which water dissociates the friction coefficient is considerably increased compared to the ideal defect-free surfaces.

and non-reactive defects. On the one hand, non-reactive defects (GRA-SW and BN-2x2C) have a negligible influence on friction. In particular, we surprisingly could not detect a significant effect of the large scale corrugation of the graphene sheet induced by the Stone-Wales defect.[48] Similarly the error bars between pristine BN and BN-2x2C overlap, so that the apparent decrease in friction induced by 2C defects is not significant [i]. On the other hand, reactive defects (GRA-V1, GRA-2H and BN-2H) cause a significant increase in friction, up to a factor of 8 for the GRA-2H defect [ii]. Among the reactive defects, there is an unexpected contrast between the vacancy and the 2H defects, despite the similar size of the protrusion induced by the dissociated water molecule.

In order to understand these results, we investigated how the different defect types modified the structure of the interface. On non-reactive defects, we did not detect any significant change in the interfacial water structure. In contrast, reactive defects profoundly modified the interactions between the water film and the surface, because of the dissociated water molecule. In particular, we analyzed the dynamics of hydrogen bonds between reactive defects and liquid water molecules, using a standard geometric criterion[56] (Fig. 3). We focused on the strong hydrogen bonds involving the oxygen of the dissociated water molecule as a donor or acceptor, and didn't account for the weak and infrequent bonds involving carbon, boron or nitrogen. On the GRA-V1 defect, the oxygen atom of the fully dissociated water molecule can only act as a hydrogen bond acceptor, limiting the average bond number between the defect and the liquid film to *ca.* 1.1. On the GRA-2H and the BN-2H defects, the OH group of the dissociated water molecule can act both as a donor and an acceptor, leading to stronger interactions with the liquid film.[57–59] For instance the GRA-2H defect accepts *ca.* 1.1 bonds and donates *ca.* 0.9 on average, making about twice as many hydrogen bonds

---

[i]Note that the introduction of graphene patches in a BN sheet could indeed reduce friction by smoothing the energy landscape locally. Yet a naive linear combination between the friction coefficients of graphene and BN predicts a decrease in friction of ca. 4 %, well below the statistical uncertainties.

[ii]In particular, the friction on the defective GRA-V1 sheet is comparable to that on the pristine BN sheet. It is striking that the difference in electronic structure between BN and graphene has an effect on friction almost as large as a molecule protruding on top of the graphene sheet, showing how important it is to account for the quantum nature of the liquid/solid interface in order to predict accurately nanofluidic transport.
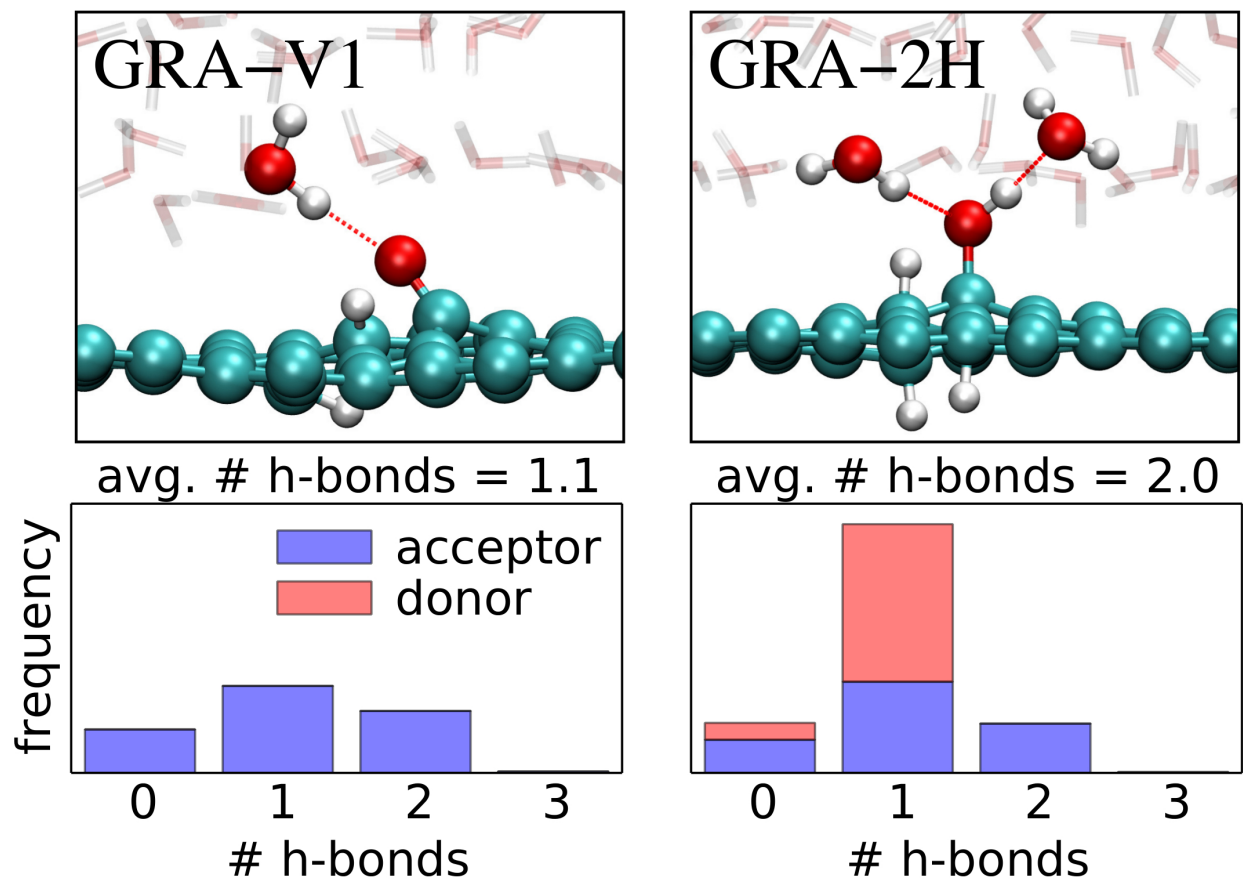
Figure 3: Top) Close-up on the interface between liquid water and two defective sheets, for the GRA-V1 (left) and GRA-2H (right) defects. After dissociating a water molecule, reactive defects form a protrusion and can hydrogen bond with the liquid; both effects lead to an increase of liquid-solid friction. Bottom) Hydrogen bonding statistics for the GRA-V1 (left) and GRA-2H (right) defects. The structure of the dissociated water molecule strongly impacts its ability to form hydrogen bonds: the oxygen atom of the fully dissociated water on the GRA-V1 defect acts only as an acceptor of hydrogen bonds, whereas the hydroxyl at the GRA-2H defect can both accept and donate hydrogen bonds with the liquid.

with the water film than the GRA-V1 defect. This points to the critical role of hydrogen bonding: indeed, the increase in friction for the GRA-2H defect is roughly twice that for the GRA-V1, which is related to the twofold increase of hydrogen bonding ability of the OH group present at 2H defects as compared to the oxygen adatom of the fully dissociated water on the vacancy.

Before discussing the consequences of these results to nanofluidic transport, we synthesize the key information gleaned from the AIMD simulations in a manner that can be extended to any defect concentration. As detailed in the SI, by identifying the effect of one defect on friction with that of a perfectly slipping hemisphere on top of the surface,[23,60] one can define an effective hydrodynamic radius R_{eff} of the defects. The friction coefficient then depends linearly on the defect surface coverage c [iii]:

$$\lambda = \lambda_0 + 2\pi\eta R_{\text{eff}}c, \tag{3}$$

where λ_0 is the friction coefficient of the defect-free surface and η the liquid viscosity. The effective radius, which controls the ratio of friction increase to defect coverage, can be deduced from the simulation results, realized at a given defect coverage $c = 1/\mathcal{A}$, where $\mathcal{A}$ is the area of the simulated interface. Using the experimental bulk water viscosity, we obtain $R_{\text{eff}} = (\lambda - \lambda_0)/(2\pi\eta c) = 84\,\text{pm}$ for the GRA-V1 defect, $170\,\text{pm}$ for the GRA-2H defect, and $104\,\text{pm}$ for the BN-2H defect.

Now that we have derived a model for the dependence of friction on defect concentration, we can come back to two of the experimental questions motivating this work. Firstly, can we expect defects appearing inevitably during the fabrication to affect interfacial friction significantly? From Eq. (3) one can estimate a critical defect coverage above which friction will increase by e.g. a factor of two: $c^{2\lambda_0} = \lambda_0/(2\pi\eta R_{\text{eff}})$. This criterion can be used to

---

[iii]Note that Eq. (3) only holds if the individual defects contributions to the friction force can be summed independently, i.e. in the dilute limit. However, a previous work has shown that the dilute-limit expression remains valid up to coverages $c_{\text{max}} \sim 0.2R_{\text{eff}}^{-2}$.[60] At defect coverages higher than c_{max} the spatial arrangement of the defects may alter the dependence of the friction coefficient.[61] However, the dilute-limit approximation should hold for the simulated systems, where $c < 0.01R_{\text{eff}}^{-2}$.

estimate if the level of defects produced by a given process is acceptable or not. For the reactive defects considered in this work, $c^{2\lambda_0}$ ranges between 0.09 (for GRA-2H defects) and $0.48\,\mathrm{nm}^{-2}$ (for BN-2H defects), corresponding roughly to 1 defect per 400 to 80 atoms. In the SI we go further and plot λ versus defect coverage for each of the reactive defects over a broad range of coverage (Fig. S5).

Secondly, when defects are desirable, *e.g.* charged groups for nanofluidic energy conversion, can we predict the energy conversion performance of a given type of defect? At the core of nanofluidic energy conversion lie the so-called electrokinetic (EK) effects, coupling different types of transport (hydrodynamic, ionic, thermal...) at interfaces.[11,15,16] EK effects are driven by surface charge, usually found in the form of charged defects at the surface. The amplitude of EK effects is therefore expected to increase with the coverage of charged defects. However EK effects are also strongly affected by interfacial hydrodynamics, and can be amplified by liquid-solid slip.[17–24] Since the extent of slip is inversely related to interfacial friction (as detailed in the SI), increasing the defect coverage will reduce slip, and hence the amplitude of EK effects. Consequently, defects are both a driving force and a hindrance for EK effects, and energy conversion performance will depend crucially on how defects modify interfacial hydrodynamics (as an example, the conversion between mechanical and electrical energy is discussed in the SI). By evaluating the effective hydrodynamic radius of different defect types, AIMD simulations can therefore be instrumental in identifying good candidates for future nanofluidic devices.

In conclusion, we have computed water friction on defective surfaces using *ab initio* molecular dynamics. Some defects do not react chemically with water, and have a negligible influence on the liquid-solid friction. Other defects dissociate water molecules. The dissociated water molecules interact strongly with the liquid water film and the liquid-solid friction increases significantly. For the range of concentrations investigated, reactive defects can increase friction up to eight times the value for pristine surfaces. Surprisingly, the increase in friction is not simply controlled by the size of the dissociated water molecule –

similar for all reactive defects. Instead it is correlated with the hydrogen bonding ability of the reactive defects, which is mainly controlled by the structure of the dissociated water molecule. Specifically we found that OH groups with which water can both accept and donate hydrogen bonds have a greater impact on friction than oxygen adatoms, with which liquid water molecules can only donate hydrogen bonds. Such detailed insight pertaining to defect chemistry, hydrogen bonding and friction would not have emerged from traditional non-dissociable force field approaches. Thus although AIMD is computationally demanding, it is a very powerful tool to investigate water-solid friction. Finally, we have shown how the information provided by AIMD can be used to estimate the performance of nanofluidic devices in the presence of defects with arbitrary surface coverage. We hope that our work will help understanding transport through real nanofluidic devices – which often suffer from reproducibility problems, and will stimulate the design of interfaces with optimal defect characteristics and concentration for applications in water treatment and sustainable energy harvesting.

Acknowledgement

Supporting Information Available

Detailed presentation of the boron nitride systems, technical details on the electronic structure setup and the molecular dynamics simulations, discussion of Green-Kubo measurements of interfacial friction in finite-size systems, presentation of a simple model defining an effective hydrodynamic radius of the defects, and discussion of the use of AIMD results to predict the energy conversion performance of defects. This material is available free of charge via the Internet at `http://pubs.acs.org/`.

References

(1) Sparreboom, W.; van den Berg, A.; Eijkel, J. C. T. Principles and applications of nanofluidic transport. *Nat. Nanotechnol.* **2009**, *4*, 713–720.

(2) Bocquet, L.; Tabeling, P. Physics and technological aspects of nanofluidics. *Lab Chip* **2014**, *14*, 3143–3158.

(3) Ma, M.; Grey, F.; Shen, L.; Urbakh, M.; Wu, S.; Liu, J. Z.; Liu, Y.; Zheng, Q. Water transport inside carbon nanotubes mediated by phonon-induced oscillating friction. *Nat. Nanotechnol.* **2015**, *10*, 692–695.

(4) Heiranian, M.; Farimani, A. B.; Aluru, N. R. Water desalination with a single-layer MoS2 nanopore. *Nat. Commun.* **2015**, *6*, 8616.

(5) Majumder, M.; Chopra, N.; Andrews, R.; Hinds, B. J. Nanoscale hydrodynamics: enhanced flow in carbon nanotubes. *Nature* **2005**, *438*, 44–44.

(6) Holt, J. K. Fast mass transport through sub-2-nanometer carbon nanotubes. *Science* **2006**, *312*, 1034–1037.

(7) Cohen-Tanugi, D.; Grossman, J. C. Water desalination across nanoporous graphene. *Nano Lett.* **2012**, *12*, 3602–3608.

(8) Siria, A.; Poncharal, P.; Biance, A.-L.; Fulcrand, R.; Blase, X.; Purcell, S. T.; Bocquet, L. Giant osmotic energy conversion measured in a single transmembrane boron nitride nanotube. *Nature* **2013**, *494*, 455–458.

(9) Murata, K.; Mitsuoka, K.; Hirai, T.; Walz, T. Structural determinants of water permeation through aquaporin-1. *Nature* **2000**, *407*, 599–605.

(10) Gravelle, S.; Joly, L.; Detcheverry, F.; Ybert, C.; Cottin-Bizonne, C.; Bocquet, L. Optimizing water permeability through the hourglass shape of aquaporins. *Proc. Natl. Acad. Sci. U. S. A.* **2013**, *110*, 16367–16372.

(11) Bocquet, L.; Charlaix, E. Nanofluidics, from bulk to interfaces. *Chem. Soc. Rev.* **2010**, *39*, 1073–1095.

(12) Bocquet, L.; Barrat, J.-L. Flow boundary conditions from nano- to micro-scales. *Soft Matter* **2007**, *3*, 685–693.

(13) Eijkel, J. Liquid slip in micro- and nanofluidics: recent research and its possible implications. *Lab Chip* **2007**, *7*, 299–301.

(14) Tocci, G.; Joly, L.; Michaelides, A. Friction of water on graphene and hexagonal boron nitride from ab initio methods: very different slippage despite very similar interface structures. *Nano Lett.* **2014**, *14*, 6872–6877.

(15) Bakli, C.; Chakraborty, S. Electrokinetic energy conversion in nanofluidic channels: addressing the loose ends in nanodevice efficiency. *Electrophoresis* **2015**, *36*, 675–681.

(16) Majumder, S.; Dhar, J.; Chakraborty, S. Resolving anomalies in predicting electrokinetic energy conversion efficiencies of nanofluidic devices. *Sci. Rep.* **2015**, *5*, 14725.

(17) Muller, V. M.; Sergeeva, I. P.; Sobolev, V. D.; Churaev, N. V. Boundary effects in the theory of electrokinetic phenomena. *Colloid Journal of the USSR* **1986**, *48*, 606–614.

(18) Joly, L.; Ybert, C.; Trizac, E.; Bocquet, L. Hydrodynamics within the electric double layer on slipping surfaces. *Phys. Rev. Lett.* **2004**, *93*, 257805.

(19) Bouzigues, C. I.; Tabeling, P.; Bocquet, L. Nanofluidics in the Debye layer at hydrophilic and hydrophobic surfaces. *Phys. Rev. Lett.* **2008**, *101*, 114503.

(20) Ren, Y.; Stein, D. Slip-enhanced electrokinetic energy conversion in nanofluidic channels. *Nanotechnology* **2008**, *19*, 195707.

(21) Morthomas, J.; Würger, A. Thermophoresis at a charged surface: the role of hydrodynamic slip. *J. Phys.: Condens. Matter* **2009**, *21*, 035103.

(22) Audry, M.; Piednoir, A.; Joseph, P.; Charlaix, E. Amplification of electro-osmotic flows by wall slippage: direct measurements on OTS-surfaces. *Faraday Discuss.* **2010**, *146*, 113–124.

(23) Joly, L.; Detcheverry, F.; Biance, A.-L. Anomalous ζ potential in foam films. *Phys. Rev. Lett.* **2014**, *113*, 088301.

(24) Maduar, S. R.; Belyaev, A. V.; Lobaskin, V.; Vinogradova, O. I. Electrohydrodynamics near hydrophobic surfaces. *Phys. Rev. Lett.* **2015**, *114*, 118301.

(25) Schmidt, T. M.; Baierle, R. J.; Piquini, P.; Fazzio, A. Theoretical study of native defects in BN nanotubes. *Phys. Rev. B* **2003**, *67*, 113407.

(26) Hashimoto, A.; Suenaga, K.; Gloter, A.; Urita, K.; Iijima, S. Direct evidence for atomic defects in graphene layers. *Nature* **2004**, *430*, 870–873.

(27) Banhart, F.; Kotakoski, J.; Krasheninnikov, A. V. Structural defects in graphene. *ACS Nano* **2011**, *5*, 26–41.

(28) Skowron, S. T.; Lebedeva, I. V.; Popov, A. M.; Bichoutskaia, E. Energetics of atomic scale structure changes in graphene. *Chem. Soc. Rev.* **2015**, *44*, 3143–3176.

(29) Pennathur, S.; Eijkel, J. C. T.; van den Berg, A. Energy conversion in microsystems: is there a role for micro/nanofluidics? *Lab Chip* **2007**, *7*, 1234–1237.

(30) Kostov, M. K.; Santiso, E. E.; George, A. M.; Gubbins, K. E.; Buongiorno Nardelli, M. Dissociation of water on defective carbon substrates. *Phys. Rev. Lett.* **2005**, *95*, 136105.

(31) Cabrera-Sanfelix, P.; Darling, G. R. Dissociative adsorption of water at vacancy defects in graphite. *J. Phys. Chem. C* **2007**, *111*, 18258–18263.

(32) Oubal, M.; Picaud, S.; Rayez, M. T.; Rayez, J. C. Interaction of water molecules with defective carbonaceous clusters: An ab initio study. *Surf. Sci.* **2010**, *604*, 1666–1673.

(33) Kaloni, T. P.; Cheng, Y. C.; Faccio, R.; Schwingenschlögl, U. Oxidation of monovacancies in graphene by oxygen molecules. *J. Mater. Chem.* **2011**, *21*, 18284–18288.

(34) Kotsalis, E. M.; Demosthenous, E.; Walther, J. H.; Kassinos, S. C.; Koumoutsakos, P. Wetting of doped carbon nanotubes by water droplets. *Chem. Phys. Lett.* **2005**, *412*, 250–254.

(35) Won, C. Y.; Aluru, N. R. Water phase transition induced by a Stone-Wales defect in a boron nitride nanotube. *J. Am. Chem. Soc.* **2008**, *130*, 13649–13652.

(36) Wei, J. W.; Zeng, H.; Pu, L. C.; Liang, J. W.; Peng, P. Electronic and optical properties of the H2O adsorbed the B-N-C nanotubes. *Eur. Phys. J. B* **2011**, *81*, 133–136.

(37) Li, X.; Li, L.; Wang, Y.; Li, H.; Bian, X. Wetting and interfacial properties of water on the defective graphene. *J. Phys. Chem. C* **2013**, *117*, 14106–14112.

(38) Striolo, A. Water self-diffusion through narrow oxygenated carbon nanotubes. *Nanotechnology* **2007**, *18*, 475704.

(39) Nicholls, W. D.; Borg, M. K.; Lockerby, D. A.; Reese, J. M. Water transport through carbon nanotubes with defects. *Mol. Simul.* **2012**, *38*, 781–785.

(40) Feibelman, P. J. Viscosity of ultrathin water films confined between aluminol surfaces of kaolinite: ab initio simulations. *J. Phys. Chem. C* **2013**, *117*, 6088–6095.

(41) VandeVondele, J.; Krack, M.; Mohamed, F.; Parrinello, M.; Chassaing, T.; Hutter, J. Quickstep: Fast and accurate density functional calculations using a mixed Gaussian and plane waves approach. *Comput. Phys. Commun.* **2005**, *167*, 103–128.

(42) Klimeš, J.; Bowler, D. R.; Michaelides, A. Chemical accuracy for the van der Waals density functional. *J. Phys.: Condens. Matter* **2010**, *22*, 022201.

(43) Zhang, C.; Wu, J.; Galli, G.; Gygi, F. Structural and vibrational properties of liquid water from van der Waals density functionals. *J. Chem. Theory Comput.* **2011**, *7*, 3054–3061.

(44) Graziano, G.; Klimeš, J.; Fernandez-Alonso, F.; Michaelides, A. Improved description of soft layered materials with van der Waals density functional theory. *J. Phys.: Condens. Matter* **2012**, *24*, 424216.

(45) Ma, J.; Michaelides, A.; Alfè, D.; Schimka, L.; Kresse, G.; Wang, E. Adsorption and diffusion of water on graphene from first principles. *Phys. Rev. B* **2011**, *84*, 033402.

(46) Al-Hamdani, Y. S.; Ma, M.; Alfè, D.; von Lilienfeld, O. A.; Michaelides, A. Communication: Water on hexagonal boron nitride from diffusion Monte Carlo. *J. Chem. Phys.* **2015**, *142*, 181101.

(47) Wu, Y.; Wagner, L. K.; Aluru, N. R. The interaction between hexagonal boron nitride and water from first principles. *J. Chem. Phys.* **2015**, *142*, 234702.

(48) Ma, J.; Alfè, D.; Michaelides, A.; Wang, E. Stone-Wales defects in graphene and other planar sp2-bonded materials. *Phys. Rev. B* **2009**, *80*, 033407.

(49) Meyer, J. C.; Kisielowski, C.; Erni, R.; Rossell, M. D.; Crommie, M. F.; Zettl, A. Direct

imaging of lattice atoms and topological defects in graphene membranes. *Nano Lett.* **2008**, *8*, 3582–3586.

(50) Pumera, M.; Wong, C. H. A. Graphane and hydrogenated graphene. *Chem. Soc. Rev.* **2013**, *42*, 5987–5995.

(51) Falk, K.; Sedlmeier, F.; Joly, L.; Netz, R. R.; Bocquet, L. Molecular origin of fast water transport in carbon nanotube membranes: superlubricity versus curvature dependent friction. *Nano Lett.* **2010**, *10*, 4067–4073.

(52) Falk, K.; Sedlmeier, F.; Joly, L.; Netz, R. R.; Bocquet, L. Ultralow liquid/solid friction in carbon nanotubes: comprehensive theory for alcohols, alkanes, OMCTS, and water. *Langmuir* **2012**, *28*, 14261–14272.

(53) Bocquet, L.; Barrat, J. L. Hydrodynamic boundary conditions, correlation functions, and Kubo relations for confined fluids. *Phys. Rev. E* **1994**, *49*, 3079–3092.

(54) Bocquet, L.; Barrat, J. L. On the Green-Kubo relationship for the liquid-solid friction coefficient. *J. Chem. Phys.* **2013**, *139*, 044704.

(55) Merabia, S.; Termentzidis, K. Thermal conductance at the interface between crystals using equilibrium and nonequilibrium molecular dynamics. *Phys. Rev. B* **2012**, *86*, 094303.

(56) Luzar, A.; Chandler, D. Hydrogen-bond kinetics in liquid water. *Nature* **1996**, *379*, 55–57.

(57) Acharya, H.; Vembanur, S.; Jamadagni, S. N.; Garde, S. Mapping hydrophobicity at the nanoscale: Applications to heterogeneous surfaces and proteins. *Faraday Discuss.* **2010**, *146*, 353–365.

(58) Giovambattista, N.; Rossky, P. J.; Debenedetti, P. G. Effect of temperature on the

structure and phase behavior of water confined by hydrophobic, hydrophilic, and heterogeneous surfaces. *J. Phys. Chem. B* **2009**, *113*, 13723–13734.

(59) Salmeron, M.; Bluhm, H.; Tatarkhanov, M.; Ketteler, G.; Shimizu, T. K.; Mugarza, A.; Deng, X.; Herranz, T.; Yamamoto, S.; Nilsson, A. Water growth on metals and oxides: binding, dissociation and role of hydroxyl groups. *Faraday Discuss.* **2009**, *141*, 221–229.

(60) Ehlinger, Q.; Joly, L.; Pierre-Louis, O. Giant slip at liquid-liquid interfaces using hydrophobic ball bearings. *Phys. Rev. Lett.* **2013**, *110*, 104504.

(61) Lee, T.; Charrault, E.; Neto, C. Interfacial slip on rough, patterned and soft surfaces: A review of experiments and simulations. *Adv. Colloid Interface Sci.* **2014**, *210C*, 21–38.